The Astrophysical Journal, 809:5 (7pp), 2015 August 10 doi:10.1088/0004-637X/809/1/5

EVIDENCE FOR NEWLY INITIATED RECONNECTION IN THE SOLAR WIND AT 1 AU

Xiaojun Xu[1,2,3], Hon-Cheng Wong[4], Yonghui Ma[1], Yi Wang[3], Meng Zhou[2], Pingbing Zuo[3], Fengsi Wei[3], Xueshang Feng[3], and Xiaohua Deng[2]
[1] Space Science Institute, Macau University of Science and Technology, Macao, China; xjxu@must.edu.mo
[2] Institute of Space Science and Technology, Nanchang University, Nanchang 330031, China
[3] SIGMA Group, Sate Key Laboratory of Space Weather, Chinese Academy of Sciences, Beijing 100190, China
[4] Faculty of Information Technology, Macau University of Science and Technology, Macao, China; hcwong@ieee.org
Received 2015 April 28; accepted 2015 June 27; published 2015 August 4

ABSTRACT

We report the first evidence for a large-scale reconnection exhaust newly initiated in the solar wind using observations from three spacecraft: *ACE*, *Wind*, and *ARTEMIS P2*. We identified a well-structured X-line exhaust using measurements from *ARTEMIS P2* in the downstream solar wind. However, in the upstream solar wind, *ACE* detected the same current sheet that corresponds to the exhaust identified by *ARTEMIS P2* data without showing any reconnection signals. We cannot find any reconnection signals from *Wind* located between *ACE* and *ARTEMIS P2*. Within the exhaust, a magnetic island is identified, which is not consistent with the quasi-steady feature as previously reported and provides further evidence that the reconnection is newly initiated. Our observations show that the entering of energetic particles, probably from Earth's bow shock, makes the crucial difference between the non-reconnecting current sheet and the exhaust. Since no obvious driving factors are responsible for the reconnection initiation, we infer that these energetic particles probably play an important role in the reconnection initiation. Theoretical analysis also shows support for this potential mechanism.

Key words: magnetic reconnection – solar–terrestrial relations – solar wind

1. INTRODUCTION

Magnetic reconnection is a fundamental process that quickly converts magnetic energy into particle energy. In the collisionless context that prevails in space plasmas, the magnetic field is frozen into the plasma. Under the frozen-in condition, magnetic reconnection is forbidden. Resistivity is required in order to break the frozen-in condition. In collisionless reconnection, its initiation requires a thin current sheet on the order of the ion inertial scale so that the kinetic effects, resulting from the decoupling of ions and electrons, can become important and play a role as a kind of resistivity (Vasyliunas 1975; Birn & Priest 2006). A computer simulation known as the "Newton Challenge" has shown that the current sheet must be thinned before the onset of reconnection (Birn et al. 2005). In the Earth's magnetosphere, reconnections have also proven to be strongly driven by the solar wind through compressing the related current sheets (Boudouridis et al. 2004). Phan et al. (2007) have demonstrated that it is compression that makes some current sheets, which show no reconnection signals in the upstream solar wind, trigger reconnection in the magnetosheath.

Until relatively recently, solar wind reconnection has rarely been studied. Gosling et al. (2005a) first proposed back-to-back Alfvénic, or slow mode, waves as direct evidence for identifying solar wind reconnection exhaust. Since then, a large number of exhausts have been reported and some new features of solar wind reconnection have been shown. First, exhausts are commonly associated with interplanetary coronal mass ejections (ICMEs; Gosling et al. 2005a, 2007b; Gosling & Szabo 2008; Phan et al. 2009; Xu et al. 2011). The low β characteristic of ICMEs is believed to be one reason for this correlation. Second, multiple spacecraft observations have suggested that reconnection in large-scale current sheets in the solar wind are generally quasi-steady with a greatly extended X-line and that the exhaust-associated current sheets are roughly planar on a large scale (Gosling 2012, and references therein). Most of the multiple spacecraft events were observed on the same side of the X-line. Only three events were observed at oppositely directed exhausts (Davis et al. 2006; Gosling et al. 2007a; Xu et al. 2011). Multiple X-lines, or magnetic islands, associated with solar wind reconnection events have not been reported to date, though they are expected. Finally, no substantial heating for either protons or electrons has been found in association with solar wind exhaust. Some of these features are different from those of reconnection in the Earth's magnetosphere, where reconnection is triggered locally. Based on the presence of extended X-lines at 1 AU, it is believed that reconnection is often initiated well inside the Earth's orbit. Phan et al. (2010) also pointed out that the reconnection occurrence rate in the solar wind could be much higher close to the Sun than at 1 AU because of the lower plasma β there. This inference that the solar wind reconnection may not have initiated locally could probably explain the different features mentioned above. However, whether reconnection could be initiated at 1 AU in the solar wind is still an open question.

Since the majority of exhausts were observed at times of decreasing or roughly constant solar wind speed, compression is not primarily responsible for producing magnetic reconnection in the solar wind (Gosling 2012). Solar wind exhausts are relatively commonly associated with thin current sheets (Gosling & Szabo 2008). It is possible for spontaneous reconnection to occur in such thin current sheets. However, the thickness of many exhausts can reach up to thousands of ion inertial lengths ($c/\omega_{\rm pi}$) (Davis et al. 2006; Xu et al. 2011; Gosling 2012). In particular, Xu et al. (2011) reported two exhausts embedded within the large-scale central current sheets of sub-flux ropes in a complex ICME. The compression between sub-flux ropes is probably responsible for the formation of these central current sheets (Owens et al. 2006;

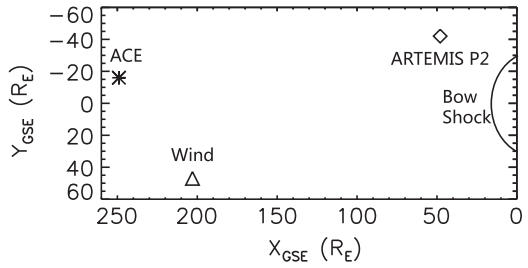

Figure 1. Sketch of the three spacecraft locations in the solar wind upstream of the Earth's bow shock and their relative positions in GSE coordinates on 2012 August 14.

Owens 2009). The long-time slowly overtaking process of the flux ropes strongly indicates that the reconnection was triggered far away from the Sun and that the reconnection could be triggered in a large-scale current sheet. Statistical studies in the solar corona have also shown that the thickness of the current sheets there is much greater than the ion inertial scale (Lin et al. 2007, 2009). Then, determining what causes the onset of reconnection in large-scale current sheets becomes a challenge in the study of reconnection. Turbulence, which can fragment the large-scale current sheets into small ones to make the kinetic effects work, has been suggested as a possible mechanism. Observations have presented reconnections in highly turbulent plasmas both in the Earth's magnetosheath (Retinò et al. 2007) and solar wind (Gosling 2007). However, such cases are very rare in the large number of reported solar wind reconnections.

In this study, we present three-spacecraft in situ evidence for a reconnection exhaust with a thickness of 130 c/ω_{pi} that was newly initiated at 1 AU in the solar wind. Our observations show that the entering of energetic particles is the main difference between the reconnection exhaust and the non-reconnecting current sheet upstream. Based on the support of theoretical analysis, we propose that energetic particles may play an important role in the reconnection initiation in large-scale weak turbulent current sheets.

2. OBSERVATIONS

On 2012 August 14, *ACE*, *Wind*, and *ARTEMIS* (standing for the mission of "Acceleration, Reconnection, Turbulence and Electrodynamics of the moon's Interaction with the Sun") P2 (Angelopoulos 2011; also known as THEMIS C) were located around [249, −16, −2.7], [203, 47, −18], and [48, −42, −4] R_E (Earth radii) in the geocentric solar ecliptic (GSE, hereafter GSE is used unless otherwise indicated) coordinates in the solar wind, respectively. As shown in Figure 1, *ACE* was in the upstream of *ARTEMIS P2* with *Wind* between them in the solar wind flow direction. In comparison with *Wind*, *ACE* and *ARTEMIS P2* were relatively much closer in the *Y* direction.

ARTEMIS P2 encountered a reconnection exhaust between 19:04:42 and 19:05:20 UT. Figure 2 shows the measurements, from the fluxgate magnetometer (FGM; Auster et al. 2008) and electrostatic analyzer (ESA; McFadden et al. 2008) on board *ARTEMIS P2*, of the exhaust. From Figure 2(a), we can see that the magnetic strength reduced 90% from 5 to 0.5 nT within the exhaust. Figures 2(b) and (c) show a pair of back-to-back Alfvén waves identified by correlated variations in $\boldsymbol{B}$ and $\boldsymbol{V}$ at the leading boundary and anticorrelated changes in $\boldsymbol{B}$ and $\boldsymbol{V}$ at the trailing boundary (Gosling et al. 2005a). A jet can be found in Figure 2(d). Although the max component of the jet is up to 40 km s^{-1} in the $+Z$ direction, it only results in a reduction of about 10 km s^{-1} in the bulk speed, which is close to the *X* component of the jet. This is because V_x was much greater than V_y and V_z and the variation of the bulk speed ($V_p = \sqrt{V_x^2 + V_y^2 + V_z^2}$) is sensitive only to ΔV_x. Since the jet was in the [+*X*, +*Y*, +*Z*] direction, the reconnection site should have been in the [−*X*, −*Y*, −*Z*] direction with respect to *ARTEMIS P2*. Other reconnection signals include enhancements of plasma density (Figure 2(e)) and temperature (Figure 2(f)). However, the temperature enhancement only occurs in the parallel direction suggesting that it probably resulted from the ion interpenetration (Gosling 2012).

By employing the minimum variance analysis of the magnetic field (MVAB) method (Sonnerup & Cahill 1967), we can perform a detailed analysis of the exhaust in the *LMN* system, where *L* is along the exhaust, *M* is along the X-line, and *N* is normal to the current sheet. The *L*, *M*, and *N* directions are calculated to be [0.28, 0.65, 0.71], [−0.20, −0.68, 0.71], and [0.94, −0.34, −0.05], respectively. Figures 3(a)–(d) show the measurements of magnetic field and plasma velocity in the *LMN* system. The total magnetic shear across the exhaust is about 160°, indicating that the reconnection is under a weak guide field. A 4 km s^{-1} shift of V_N (Figure 2(d)) across the exhaust corresponds to a 2 km s^{-1} reconnection inflow (V_{in}). Then, the dimensionless reconnection rate, V_{in}/V_A, where $V_A = 60$ km s^{-1} is the inflow Alfvén speed, is about 3.3% in the range of fast reconnection. The width of the exhaust can be calculated by V_N (= 445 km s^{-1}) timing the spacecraft crossing duration, to be 1.7×10^4 km (2.65 R_E) or 130 c/ω_{pi}.

Figure 3(e) presents the wedge angle between the magnetic field and the *L* direction. The rotation of magnetic field is very smooth across the exhaust with a very slight bifurcation only in the *L* component. It is similar to the direction rotation of a magnetic cloud that is considered to be a large-scale flux rope (Burlaga et al. 1981). Here the smoothly rotated magnetic field suggests the possible existence of a flux rope or magnetic island as previously reported by reconstruction (Teh et al. 2009) and by simulation (Wang et al. 2010) in the solar wind. Since the guide field is weak, a magnetic island is preferable in this case (Eastwood et al. 2007).

At 18:20:05–18:21:00 UT, the *ACE* spacecraft observed the same current sheet in the upstream solar wind. This time interval of 45 minutes is in good agreement with the propagating time of the solar wind from *ACE* to *ARTEMIS P2* along the *X* direction. Since the reconnection site was in the [−*X*, −*Y*, −*Z*] direction of *ARTEMIS P2* as pointed out above and *ACE* was located in the [+*X*, +*Y*, +*Z*] direction of *ARTEMIS P2*, these two spacecraft should be at the same side of the reconnection X-line. Figure 4 shows the measurements of plasma and magnetic field by *ACE*. However, the current sheet detected by *ACE* shows no reconnection signals. There is no apparent plasma jet in the bulk speed or in any velocity component. The *L* direction of the current sheet is [0.07, 0.86, 0.51], i.e., mainly along the *Y* axis, which is consistent with the most field rotation in the *Y* direction. However, no enhancement of V_y and no correlated/anticorrelated variations in the dominant B_y and V_y at the boundaries of the current sheet have been detected. The velocity measured by the *ACE*/SWEPAM-I instrument has a 64 s resolution. A complete 64 s measurement cycle is comprised of five 12.8 s measurement segments with each segment containing eight E/Q levels. The first

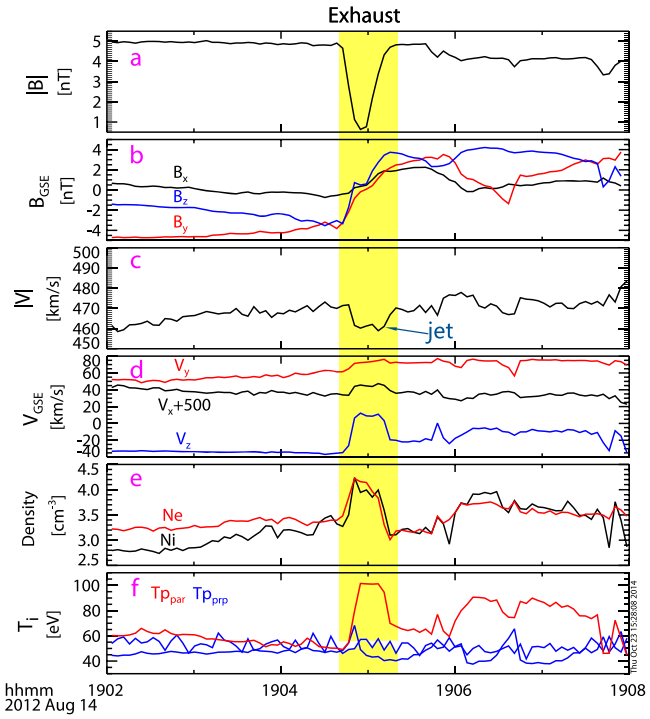

Figure 2. *ARTEMIS P2* measurements of magnetic field and plasma around the exhaust. (a) Magnetic strength. (b) Magnetic field vector. (c) Plasma bulk speed showing an apparent jet. (d) Plasma velocity. (e) Ion density (black) and electron density (red). (f) Field-aligned ion temperatures with obvious enhancement in the parallel component. The exhaust is in the yellow box.

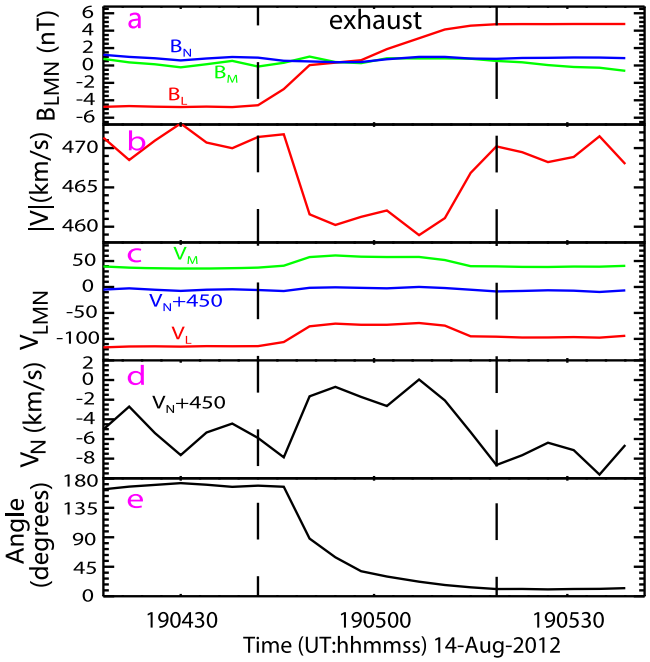

Figure 3. Analysis around the exhaust in the *LMN* coordinates. (a) The magnetic field in the *LMN* system. (b) Plasma bulk speed. (c) Plasma velocity in the *LMN* system, a jet of ~50 km s^{-1} occurring in the *L* direction within the exhaust. (d) Zoom-in of V_N. (e) The wedge angle between the magnetic field and the *L* direction along the crossing trajectory.

measurement segment starts with the level $L_{mx}-25$, where L_{mx} represents the maximum counting rate and the time tag of the measurement cycle is placed 16 s after the first measurement (McComas et al. 1998). In our case, the time tag of the

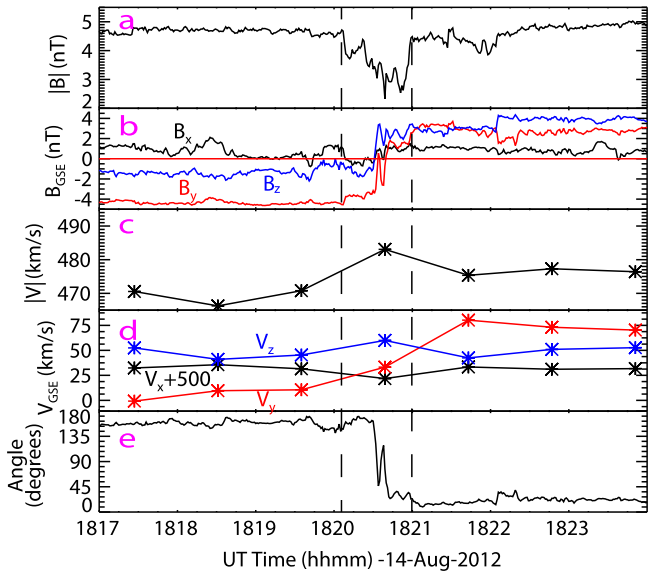

Figure 4. Measurements of the current sheet by *ACE* showing no reconnection signals. (a) Magnetic field strength. (b) The magnetic field vector. (c) Plasma bulk speed: no plasma jet within the current sheet. (d) The velocity: no obvious enhancement in any component of the velocity. (e) The wedge angle between the field line with the *L* direction. The two vertical dashed lines mark the boundaries of the current sheet.

measurement within the exhaust was at 18:20:39, indicating that the first measurement started at 18:20:23 and level L_{mx} was measured at 18:21:01, which is almost at the trailing edge of the current sheet. That means the measurement within the current sheet contains all of the portions with energies less than level L_{mx} and the rest of the higher energy portions from the trailing inflow region. If there existed a $+Y$ jet within the current sheet, the V_y within the current sheet should have been larger than that from the trailing inflow region, because it should have a harder low energy spectrum and a similar high energy spectrum. In fact, exhausts have been observed down to the limit of measurement cadence (Gosling 2012). Therefore, although there was only one measurement, we can still verify that there was no jet within the current sheet. Besides, compared with the smooth rotation of the exhaust, the complete reversal of the current sheet field direction is much steeper (Figure 4(e)). Furthermore, the decrease of field strength in the current sheet is only 47% (from 4.7 to 2.5 nT), which is much less than that in the exhaust. It is similar to the study of Phan et al. (2007), in which the field strength reduction in the non-reconnecting solar wind current sheet is also much less than that in the reconnection layer that is initiated in the magnetosheath.

Meanwhile, *Wind* was located between (much closer to) *ACE* and *ARTEMIS P2*. We show the measurements of *Wind* during the time interval only from 18:20:00 to 18:50:00 UT in Figure 5. It can be basically assured that this time interval contains all of the solar wind observations that are possibly related to the exhaust. However, from Figure 5, we can see that the changes of the magnetic field and velocity are continuously and consistently correlated throughout this time interval. This positive correlation is especially obvious in both *Y* and *Z* components. We cannot find any well-structured current sheet that corresponds to either the current sheet by *ACE* or the exhaust by *ARTEMIS P2*. We also cannot identify any reconnection exhaust from the *Wind* measurements during this

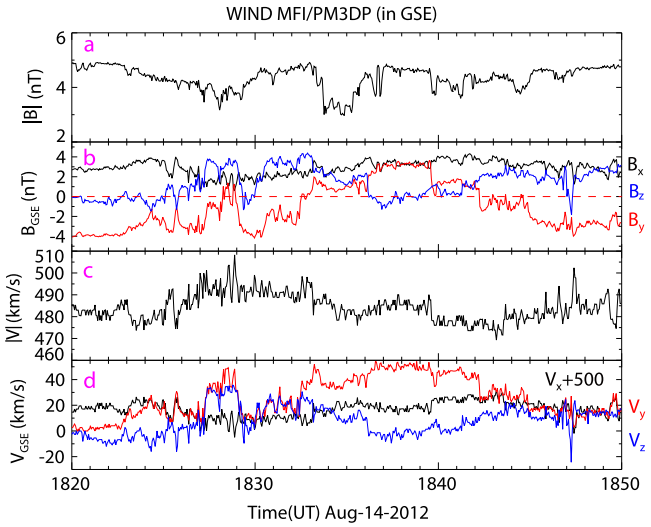

Figure 5. *Wind* measurements of magnetic field and plasma during the time interval associated with the current sheet observed by *ACE* and *ARTEMIS P*2. (a) Magnetic strength. (b) Magnetic field vector. (c) Plasma bulk speed. (d) Plasma velocity vector. The changes of $\boldsymbol{B}$ and $\boldsymbol{V}$ maintain an accordant correlated variation throughout the entire time interval. This feature is especially obvious in the *Y* and *Z* components. No reconnection exhaust has been identified during this time interval.

time interval. The distance from *ACE* to *Wind* is calculated to be $\sim 0.5 \times 10^6$ km. The average correlation length of magnetic strength ($\lambda_{|B|}$) at solar minimum is about 0.75×10^6 km (Wicks et al. 2010). Considering that the solar activity in 2012 was relatively low and taking the statistical error into account, this separation is roughly near the low limit of the average correlation length. Since no large-scale disturbances, such as shock, ICME, and heliospheric current sheet, have been identified between *ACE* and *Wind*, it is thus possible that the current sheet just happened to disappear within the distance mainly along the *Y* direction.

Since *ACE* and *Wind* were much more separated in the *Y* direction than in the *X* direction, the tilt of the current sheet may result in the possibility that *Wind* observed the current sheet or exhaust prior to *ACE*. In fact, *Wind* indeed observed an exhaust around 18:01 UT. Figure 6 shows the exhaust, which is represented by the yellow box. We calculated the normals of the exhausts at both *ACE* and *Wind* to test whether the time delay between them can result from the tilt of the current sheet. First, the displacement vector between *ACE* and *Wind* ($\boldsymbol{r}_{\rm AW}$) can easily be derived. Then, we can get the displacement along the normal of the current sheet plane ($r_n = \boldsymbol{r}_{\rm AW} \cdot \boldsymbol{n}$, where $\boldsymbol{n}$ is the normal). After that, once we get the normal speed of the current sheet plane ($V_n = \boldsymbol{V} \cdot \boldsymbol{n}$, where $\boldsymbol{V}$ is the current sheet velocity), we can calculate the time delay from *ACE* to *Wind* ($\Delta t = r_n/V_n$). Taking a particular case, $\boldsymbol{n} = [1, 0, 0]$, for example, $\boldsymbol{r}_{\rm AW} = [46, -63, 15.3]$ and $\boldsymbol{V} = [-475, 50, 50]$, then the predicted time delay is −10.3 minutes. It is obvious that in this particular case, *ACE* must be prior to *Wind*. Therefore, minus predicted time delays indicate that *ACE* is prior to *Wind* and this result is independent of the direction of $\boldsymbol{n}$. The predicted time delays are shown in Table 1. Both results show that *ACE* should be prior to *Wind* to detect the current sheet. However, the exhaust around 18:01 UT at *Wind* is 20 minutes prior to that at *ACE* (18:21 UT). Taking into consideration the ∼10-minute time delay between *ACE* and *Wind*, this error of more than 20 minutes is too large. In comparison, the predicated time delays between *ACE* and *ARTEMIS*, calculated from the normals of current sheets at both *ACE* and *ARTEMIS P*2, are shown in Table 2. They are in very good agreement and the observed time delay is −45 minutes. Note that the separation between *ACE* and ARTEMIS in the *Y* direction is also 26 $R_{\rm E}$ which is up to 41% of that between *ACE* and *Wind*. Therefore, we conclude that the exhaust *Wind* detected at 18:01 UT is not the same one that *ACE* observed at 18:21 UT. This means that no reconnection structure corresponding to the exhaust at *ARTEMIS P*2 can be identified from *Wind* measurements.

When the current sheet moved downstream, the solar wind speeds across the current sheet from both *ACE* and *ARTEMIS P*2 measurements varied only slightly. In other words, there is no strong local compression to drive the reconnection. Long-time observations from *ACE* show that the speed of solar wind gradually decreased from August 13 12:00 UT to August 15 24:00 UT (not shown), suggesting that no strong large-scale compression would be expected. However, an important difference between observations from *ACE* and *ARTEMIS P*2 is the entering of energetic particles with energies of up to 100 keV for ions and 2 keV for electrons into the current sheet. Figure 7 shows the calibrated fluxes and pitch angle distributions (PAD) of energetic ions and suprathermal electrons around the current sheet/exhaust by *ACE*/SWEPAM and the solid state telescope (SST; Angelopoulos 2008) on board *ARTEMIS P*2. When *ACE* crossed the current sheet, there were no flux enhancements of energetic ions and electrons as shown in Figure 7(a). However, *ARTEMIS P*2 observed substantial increases of energetic ions and electrons. Figure 7(b) shows that the omnidirectional fluxes of energetic ions observed by *ARTEMIS P*2 were greatly increased. Figure 7(c) further shows the PAD of these energetic ions. From Figure 7(d), we can see long-time continuous suprathermal electrons that centered at 180° before and after the exhaust. These strahl electrons were moving antiparallel to the field from the Sun. Figure 7(c) shows that energetic ions were moving parallel to the field, which indicates that they were moving sunward. Since energetic ions from the Earth's bow shock can frequently move upstream in the solar wind (Lin et al. 1974), they are most probably from the Earth's bow shock. The magnetic field direction at *ARTEMIS P*2 when the energetic ions were observed was about [−0.5, −3.0, −3.0]. Although it seems that such field lines were not radially connected with the bow shock, it is still possible for the bow shock origin energetic particles to reach *ARTEMIS P*2 by indirect magnetic connections as pointed out by Haggerty et al. (2000). However, the different origins of these energetic ions and electrons will actually not affect the main conclusion of this study.

The dropout of electron strahls within the exhaust in Figure 7(d) indicates the change of magnetic connectivity with the Sun (Gosling et al. 2005b; Gosling et al. 2006). It should be pointed out that such a dropout of electron strahls did not happen in the *ACE* 272 eV measurements (not shown). Since the dropouts of electron strahl can be a result of isotropization (Pagel et al. 2005) or field lines with very long connection to the Sun (Owens & Crooker 2007), the field lines without strahl electrons could still be connected to the Sun through a different connection. We here use "directly connected with Sun" to describe the field lines with strahl electrons, whereas we use "not directed connected with Sun" to

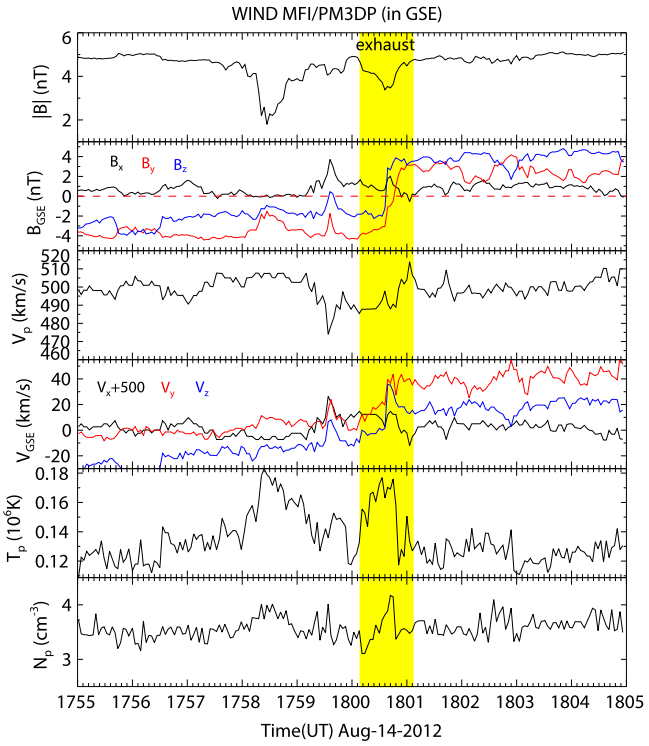

Figure 6. *Wind* observations of a reconnection exhaust at 18:01 UT, which was much prior to *ACE*. (a) Magnetic strength. (b) Magnetic field vector. (c) Plasma bulk speed. (d) Plasma velocity vector. (e) Ion temperatures. (f) Ion density.

Table 1
Predicted Time Delays between *ACE* and *Wind*

S/C	Normal	Predicted Time Delay (Minutes)
ACE	[0.88, 0.15, −0.45]	−5.93
Wind	[0.84, 0.40, −0.36]	−2.12

Table 2
Predicted Time Delays between *ACE* and *ARTEMIS P2*

S/C	Normal	Predicted Time Delay (Minutes)
ACE	[0.88, 0.15, −0.45]	−42
P2	[0.94, −0.34, −0.05]	−45.1

indicate those field lines without strahl electrons. As illustrated in Figure 8, further evidence for the existence of the magnetic island is provided. As marked by Lines "I" and "IV" in Figure 8, the field lines of the leading and trailing inflow regions are directly connected with the Sun and the suprathermal electrons move antiparallel to the field. If all the field lines after reconnection are open in the exhaust, such as Field Line "II," one would have expected to observe an antiparallel directed strahl throughout the exhaust. The reason for this is that reconnection can only cut off the direct magnetic connection with the Sun of the field lines from the leading inflow region while the field lines from the trailing inflow region are still directly connected. Instead, the magnetic topology of the magnetic island is in good agreement with the different magnetic connectivity to the Sun from both inflow regions. The formation of the magnetic island probably resulted from multiple X-point reconnection or a magnetic island

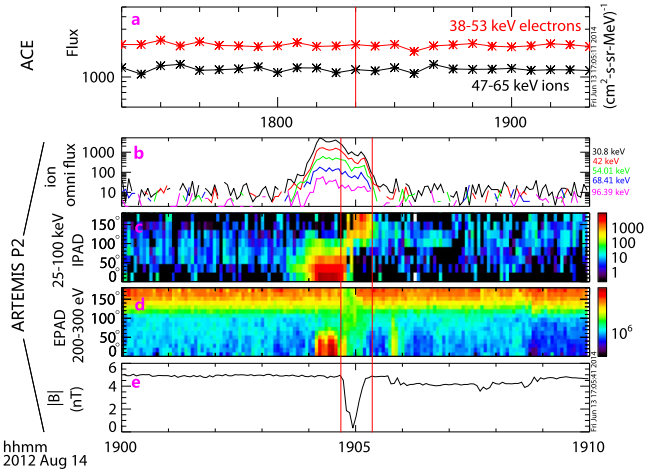

Figure 7. Fluxes and pitch angle distributions of energetic ions and suprathermal electrons around the same current sheet. (a) Energetic ion and electron measurements by *ACE* with no reconnection signals. The red vertical line marks the current sheet. (b) The omnidirectional differential fluxes of energetic ions from 30 to ~100 keV, showing great enhancements in the exhaust. (c) The pitch angle distribution of energetic ions. (d) The pitch angle distribution of suprathermal electrons between 200 and 300 eV measured by *ARTEMIS P2* around the exhaust. (e) The magnetic strength as a reference of the exhaust. The two red lines indicate the boundaries of the exhaust. All the differential fluxes measured by *ARTEMIS P2* are in units of eV/(cm^2-sec-sr-eV).

produced by reconnection. The magnetic island can also explain the isotropic distribution of energetic ions related to the absence of electron strahls. The field line radius of the curvature of the magnetic island is on the same order of thickness as the current sheet and thus is less than the Larmor radius of the energetic ions. When the Larmor radius of the energetic ions is larger than the curvature of the magnetic field lines, these ions will perform an isotropic distribution rather than parallel or antiparallel distribution. However, the magnetic island does not fill the entire exhaust, suggesting that it probably was a secondary island produced in the vicinity of the reconnection X-line and ejected outwards (Eastwood et al. 2007). Previous reports have shown that all of the solar wind reconnections identified by multiple spacecraft observations are quasi-steady (Davis et al. 2006; Phan et al. 2006; Gosling et al. 2007a; Xu et al. 2011). However, the magnetic island here provides evidence for time-dependent reconnection in the solar wind. The solar wind reconnection would probably undergo a time-dependent process before reaching its quasi-steady state.

It should be noted that the observable features of flux rope or magnetic island produced by reconnection in the solar wind are probably unlike those in the Earth's magnetosphere. Since the spacecraft usually crosses the solar wind exhaust mainly along the normal direction, it cannot observe a bipolar feature of the normal component, which is crucial evidence for identifying a flux rope or magnetic island in magnetospheric reconnection. Besides, even a flux rope may not show much enhanced core magnetic field strength with respect to the ambient plasmas in the solar wind. The reason is that, due to the relatively low spatial resolution of solar wind measurements, the ambient plasmas are usually outside of the current sheet. Furthermore, it is not surprising that the field strength in the current sheet is weaker than the field strength outside of it even when there is a flux rope. The situation in the Earth's magnetosphere is quite

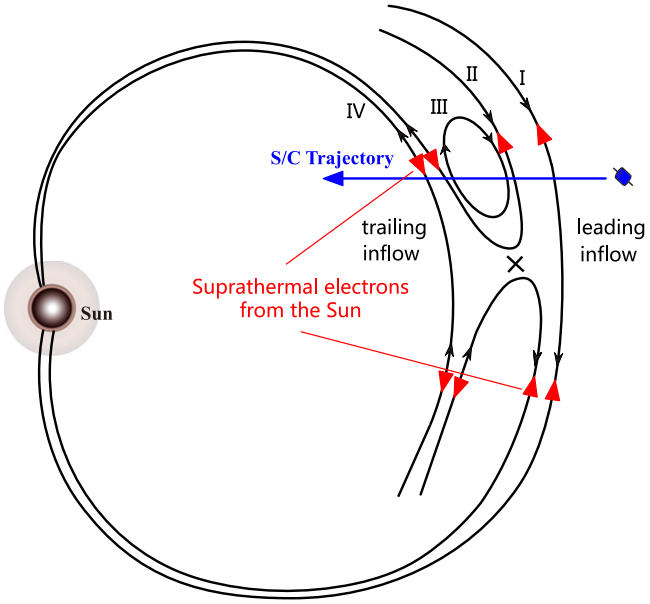

Figure 8. Illustration of direct magnetic connectivity with the Sun and the distributions of electron strahls in different portions of the reconnection structure. In this study, the field lines, marked by "I" and "IV," of both inflow regions are directly connected to the Sun with strahl electrons moving antiparallel to the field. Line "II" indicates the open field lines in the exhaust. Line "III" indicates closed field lines in the exhaust, which are not directly connected with the Sun resulting in the dropout of electron strahls. It is important to note that this is a 2D sketch of a 3D configuration. Field lines of type "III" may still be connected to the Sun by the "out-of-plane" component. However, the connection could be very complex, which we refer to as "not directly connected with Sun."

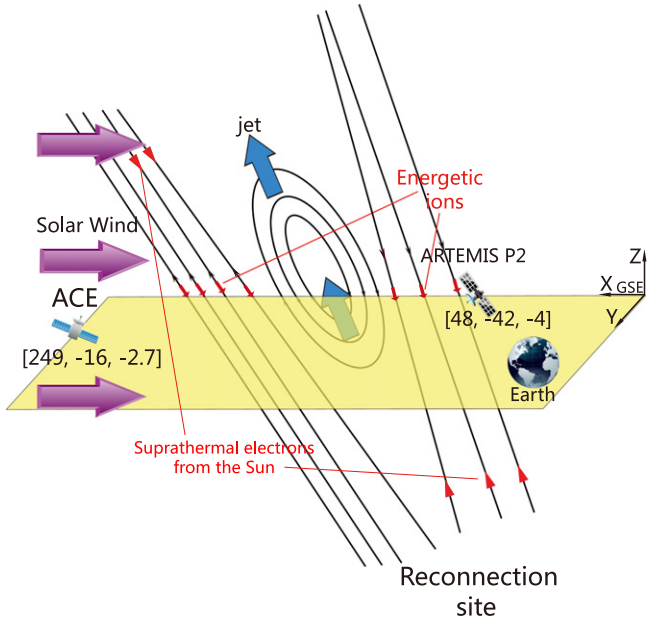

Figure 9. Overview of the entire event in this study. *ARTEMIS P2* observed a reconnection exhaust while *ACE* observed a corresponding current sheet with no reconnection signals in the upstream solar wind. The existence of a magnetic island within the exhaust is strongly indicated by electron strahls distributions.

different. Because of the very high spatial resolution there, the ambient plasmas (with respect to the flux rope) are also in the vicinity of the neutral line. Thus the enhancement of core field strength of the flux rope can be clearly verified.

3. DISCUSSIONS AND CONCLUSIONS

During the propagation of the current sheet from *ACE* to *ARTEMIS P2*, no obvious driving factors for reconnection are found besides the slight compression. Turbulence is believed to be an important factor for the triggering of reconnection in large-scale current sheets by fragmenting the current sheet into small ones. However, in this study, the turbulence is not strong enough for the formation of small-scale current sheets (Retinò et al. 2007). Some other mechanisms are required. The frozen-in condition for the ideal plasma is described as $\boldsymbol{E} + \boldsymbol{v} \times \boldsymbol{B} = 0$, where $\boldsymbol{E}$ is the electric field, $\boldsymbol{B}$ is the magnetic field, and $\boldsymbol{v}$ is the plasma bulk velocity. We should note that, at any specific time and place, the $\boldsymbol{E}$ and $\boldsymbol{B}$ are unique values while the velocity is actually a distribution. In most general situations, the flux of energetic particles is low and they move field-aligned, so they cannot efficiently affect the frozen-in condition. However, in this study, the number of energetic ions could be much greater than that in the normal distribution and a significant part of them are non-field-aligned (Figure 7(c)). If the bulk velocity (say $\boldsymbol{v}_{\rm b}$) satisfies the frozen-in condition, then these energetic ions with a different velocity from $\boldsymbol{v}_{\rm b}$ can naturally generate a resistivity to break the frozen-in condition while without requiring the current sheet to be thin enough. Energetic ions upstream of the Earth's bow shock are proven to be able to produce different kinds of waves including whistler waves (Fairfield 1974; Anderson et al. 1981), which have been observed just before reconnection initiation in the Earth's magnetotail (Wei et al. 2007). This kind of resistivity to break the frozen-in condition could exist in the form of wave-particle interaction. Unfortunately, because *ARTEMIS P2* was not working in the burst mode, the wave activity can hardly be seen in the low resolution data in this study.

The fact that collisionless magnetic reconnection is driven and mediated by whistler waves (Mandt et al. 1994) has been proven by in situ observations (Deng & Matsumoto 2001). In the whistler regime, the electrons carry the currents while the ions provide a neutralizing background. The electron MHD equation (Kingsep et al. 1990) without the resistive term is $\frac{\partial \boldsymbol{B}}{\partial t} + \frac{1}{ne}\nabla \times \boldsymbol{j} \times \boldsymbol{B} = 0$, where n is the plasma density and e is the elementary charge. The current $\boldsymbol{j}$ is derived by neglecting the motion of ions, which requires that the system scale is less than 10 $c/\omega_{\rm pi}$ so that the motions of ions and electrons can decouple. Computer calculations show that the second term of the equation can generate the whistler waves that drive and mediate the collisionless reconnection (Mandt et al. 1994). However, the suprathermal electron beams from the Sun can also generate whistler waves. In the turbulent solar wind plasma, the suprathermal electron beams carry currents ($\boldsymbol{j}_{\rm eb}$) themselves, but without requiring the decoupling of ions and electrons in thin current sheets. If the magnetic field is weakly turbulent, $\nabla \times \boldsymbol{j}_{\rm eb} \times \boldsymbol{B}$ can be significantly non-zero. Solar wind exhausts show a high occurrence rate in association with ICMEs (Gosling et al. 2007b), where suprathermal electron beams are common. However, if the magnetic field is highly turbulent, $\boldsymbol{j}_{\rm eb} \times \boldsymbol{B}$ is isotropic and $\nabla \times \boldsymbol{j}_{\rm eb} \times \boldsymbol{B}$ is still zero. Maybe that is one reason why reconnection exhaust is very rare in the highly turbulent high-speed solar wind (Gosling 2007).

In summary, in situ observations of three spacecraft provide evidence for a newly initiated reconnection in the solar wind.

Figure 9 shows the overview of this event. A large-scale current sheet with no reconnection signals was first observed by *ACE*. Due to several factors, such as the field lines not being connected with the bow shock or the distance being too far, energetic particles were not observed by *ACE*. This current sheet most likely had not extended to the location of *Wind*, and thus it was not observed by *Wind*. Sometime during its propagation to Earth, energetic particles began to enter into the current sheet along the field lines, and, finally, a reconnection exhaust associated with the energetic particles was detected by *ARTEMIS P2*. We infer that energetic particles may play an important role in the initiation of solar wind reconnection in large-scale current sheets. In addition, theoretical analysis also gives support for this potential mechanism. Since there are a lot of energetic particles in the solar corona, they may also play a role in the initiation of near-synchronous long-distance flares and eruptions with magnetic connections (Schrijver & Title 2011). However, we actually have no observable information about the real process that happened at the reconnection site when reconnection was being triggered. Further observations, quantitative analysis, and computer simulations are required.

We thank J. T. Gosling for many helpful discussions. This work is supported by the Science and Technology Development Fund of Macao SAR (080/2012/A3), the National Natural Science Foundation of China (NSFC) under grants 41204123, 41374174, 41231068, and 41331070, and the Science Foundation of Jiangxi Province under grant 20144BAB2110005. We acknowledge NASA contract NAS5-02099 and V. Angelopoulos for use of data from the THEMIS Mission. Specifically, we thank C. W. Carlson and J. P. McFadden for use of ESA, K. H. Glassmeier, U. Auster, and W. Baumjohann for use of FGM data, and D. Larson and R. P. Lin for use of SST data. We also thank *ACE* and *Wind* teams and NASA CDAWeb for providing the data.

REFERENCES

Anderson, R. R., Parks, G. K., Eastman, T. E., Gurnett, D. A., & Frank, L. A. 1981, JGRA, 86, 4493
Angelopoulos, V. 2008, SSRv, 141, 5
Angelopoulos, V. 2011, SSRv, 165, 3
Auster, H. U., Glassmeier, K. H., Magnes, W., et al. 2008, SSRv, 141, 235
Birn, J., Galsgaard, K., Hesse, M., et al. 2005, GeoRL, 32, L06106
Birn, J., & Priest, E. R. 2006, Reconnection of Magnetic Fields: Magnetohydrodynamics and Collisionless Theory and Observations (New York: Cambridge Univ. Press)
Boudouridis, A., Zesta, E., Lyons, L. R., Anderson, P. C., & Lummerzheim, D. 2004, AnGeo, 22, 1267
Burlaga, L., Sittler, E., Mariani, F., & Schwenn, R. 1981, JGRA, 86, 6673
Davis, M. S., Phan, T. D., Gosling, J. T., & Skoug, R. M. 2006, GeoRL, 33, L19102
Deng, X. H., & Matsumoto, H. 2001, Natur, 410, 557
Eastwood, J. P., Phan, T.-D., Mozer, F. S., et al. 2007, JGRA, 112, A06235
Fairfield, D. H. 1974, JGR, 79, 1368
Gosling, J. T. 2007, ApJL, 671, 73
Gosling, J. T. 2012, SSRv, 172, 187
Gosling, J. T., Eriksson, S., Blush, L. M., et al. 2007a, GeoRL, 34, L20108
Gosling, J. T., Eriksson, S., Blush, L. M., et al. 2007b, JGRA, 112, A08106
Gosling, J. T., McComas, D. J., Skoug, R. M., & Smith, C. W. 2006, GeoRL, 33, L17102
Gosling, J. T., Skoug, R. M., McComas, D. J., & Smith, C. W. 2005a, JGRA, 110, A01107
Gosling, J. T., Skoug, R. M., McComas, D. J., & Smith, C. W. 2005b, GeoRL, 32, L05105
Gosling, J. T., & Szabo, A. 2008, JGRA, 113, A10103
Haggerty, D. K., Roelof, E. C., Smith, C. W., et al. 2000, JGRA, 105, 25123
Kingsep, A. S., Chukbar, K. V., & Yankov, V. V. 1990, in Reviews of Plasma Physics, Vol. 16, ed. B. B. Kadotsmev (New York: Consultants Bureau), 243
Lin, J., Li, J., Forbes, T. G., et al. 2007, ApJL, 658, 123
Lin, J., Li, J., Ko, Y.-K., & Raymond, J. C. 2009, ApJ, 693, 1666
Lin, R. P., Meng, C.-I., & Anderson, K. A. 1974, JGR, 79, 489
Mandt, M. E., Denton, R. E., & Drake, J. F. 1994, GeoRL, 21, 73
McComas, D. J., Bame, S. J., Barker, P., et al. 1998, SSRv, 86, 563
McFadden, J. P., Carlson, C. W., Larson, D., et al. 2008, SSRv, 141, 277
Owens, M. J. 2009, SoPh, 260, 207
Owens, M. J., & Crooker, N. U. 2007, JGRA, 112, A06106
Owens, M. J., Merkin, V. G., & Riley, P. 2006, JGRA, 111, A03104
Pagel, C., Crooker, N. U., Larson, D. E., et al. 2005, JGRA, 110, A01103
Phan, T. D., Drake, J. F., Shay, M. A., Mozer, F. S., & Eastwood, J. P. 2007, PhRvL, 99, 255002
Phan, T. D., Gosling, J. T., & Davis, M. S. 2009, GeoRL, 36, L09108
Phan, T. D., Gosling, J. T., Davis, M. S., et al. 2006, Natur, 439, 175
Phan, T. D., Gosling, J. T., Paschmann, G., et al. 2010, GeoRL, 40, 11
Retinò, A., Sundkvist, D., Vaivads, A., et al. 2007, NatPh, 3, 235
Schrijver, C. J., & Title, A. M. 2011, JGRA, 116, A04108
Sonnerup, B. U. Ö, & Cahill, L. J., Jr. 1967, JGR, 72, 171
Teh, W.-L., Sonnerup, B. U. Ö, Hu, Q., & Farrugia, C. J. 2009, AnGeo, 27, 807
Vasyliunas, V. M. 1975, RvGeo, 13, 303
Wang, Y., Wei, F. S., Feng, X. S., et al. 2010, PhRvL, 105, 195007
Wei, X. H., Cao, J. B., Zhou, G. C., et al. 2007, JGRA, 112, A10225
Wicks, R. T., Owens, M. J., & Horbury, T. S. 2010, SoPh, 262, 191
Xu, X., Wei, F., & Feng, X. 2011, JGRA, 116, A05105